~~CONFIDENTIAL~~

Copy 44
RM SL54F17

NACA RM SL54F17

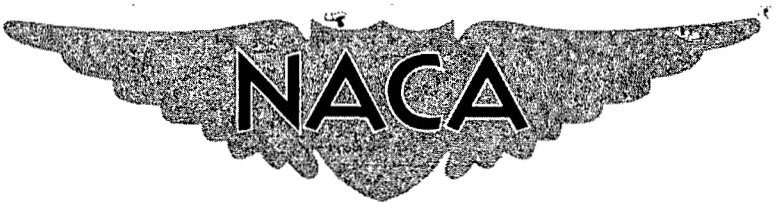

RESEARCH MEMORANDUM

for the

Bureau of Aeronautics, Department of the Navy

MINIMUM DRAG OF 0.11-SCALE ROCKET-POWERED MODELS OF THE CHANCE VOUGHT XF8U-1 AIRPLANE, WITH AND WITHOUT NOSE MODIFICATIONS, AT MACH NUMBERS BETWEEN 0.85 AND 1.30

TED NO. NACA DE 392

By Willard S. Blanchard, Jr.

Langley Aeronautical Laboratory
Langley Field, Va.

CLASSIFIED DOCUMENT

NATIONAL ADVISORY COMMITTEE
FOR AERONAUTICS

WASHINGTON

~~CONFIDENTIAL~~

NACA RM SL54F17

NATIONAL ADVISORY COMMITTEE FOR AERONAUTICS

RESEARCH MEMORANDUM

for the

Bureau of Aeronautics, Department of the Navy

MINIMUM DRAG OF 0.11-SCALE ROCKET-POWERED MODELS OF THE CHANCE VOUGHT XF8U-1 AIRPLANE, WITH AND WITHOUT NOSE MODIFICATIONS, AT MACH NUMBERS BETWEEN 0.85 AND 1.30

TED NO. NACA DE 392

By Willard S. Blanchard, Jr.

SUMMARY

Drag data obtained from the flight tests of two 0.11-scale rocket-powered models of the Chance Vought XF8U-1 airplane are presented herein. The data were obtained over a Mach number range between 0.85 and 1.30 and at Reynolds numbers between 6.5×10^6 and 11.5×10^6, respectively. Also included is the variation of trim lift coefficient with Mach number, based on unpublished tunnel data, corrected to the center-of-gravity location of the models of this investigation.

Minimum drag coefficient of the first (original) configuration increased from about 0.0175 at $M = 0.9$ to about 0.0445 at $M = 1.1$, then decreased slightly to about 0.0440 at $M = 1.285$. For the second (modified nose) configuration, the corresponding values were 0.0185, 0.0420, and 0.0410. For both configurations, the drag-rise Mach number (based on $dC_D/dM = 0.10$) was 0.93. The nose modifications resulted in a decrease of about 0.0035 in the pressure-drag coefficient at Mach numbers between 1.1 and 1.285.

INTRODUCTION

At the request of the Bureau of Aeronautics, Department of the Navy, the Langley Pilotless Aircraft Research Division is conducting an investigation of the low-lift drag of the Chance Vought XF8U-1 airplane. The models employed in the tests are 0.11-scale and are rocket-boosted to supersonic speeds.

The XF8U-1 is a jet-propelled, swept-wing, fighter-type airplane designed to fly at supersonic speeds. The airplane is conventional in general geometry, and utilizes an all-movable horizontal tail for longitudinal trim and control. The duct inlet is an underslung scoop located near the nose.

The purpose of the tests reported herein was to obtain low-lift drag at transonic and low supersonic speeds of the complete airplane in the clean, high-speed configuration, with and without a modified forebody. The nose modification consisted of a slimmer canopy, a slimmer nose generally, and a sharper duct inlet lip.

SYMBOLS

M	free-stream Mach number
R	Reynolds number, based on mean aerodynamic chord
W	model weight, 148.4 lb and 142.2 lb for models 1 and 2, respectively
$\bar{c}$	mean aerodynamic chord, 1.295 ft
q	free-stream dynamic pressure, lb/sq ft
S	model wing area (leading and trailing edges extended to fuselage center line), 4.55 sq ft
C_D	drag coefficient, Drag/qS
V	velocity, ft/sec
t	time, sec
γ	flight-path angle, deg
p	free-stream static pressure, lb/sq ft

ρ	density of air, slugs/cu ft
A	cross-sectional area, sq ft; also, aspect ratio
l	model length from nose to fuselage base, 5.58 ft and 5.62 ft for models 1 and 2, respectively
r	radius, ft
x	distance rearward from model nose, ft
g	acceleration due to gravity, value taken as 32.2 ft/sec^2

MODELS

Figure 1 is a three-view drawing of the basic model used in this investigation; figures 2 to 4 show model cross-sectional area plotted against fuselage station for models 1 and 2; figures 5 to 8 are photographs of the models. Presented in table I are geometric dimensions of the two models.

Each model was built around a $3\frac{1}{2}$-inch-diameter steel thrust tube which extended from ahead of the leading edge of the wing root to the base of the fuselage. The wing was bolted directly to this tube. The fuselage was of mahogany. The wing and tails were of solid aluminum alloy.

In order to facilitate radar tracking, a smoke-tank was built into the fuselage of each model. Smoke provided in this manner afforded a visible trail which commenced when the model separated from the booster rocket.

Model 1 was the basic configuration of the proposed airplane. Model 2 had a modified forebody - an attempt to reduce the supersonic drag level. The modifications consisted of a smaller canopy, a slimmer and slightly longer forebody with a sharper nose, and a sharper duct inlet lip. The effect of these modifications on the area distribution can be seen in figure 4. In figures 5 to 8, which are photographs of models 1 and 2, the visible change in geometry of the forebody brought about by the nose modifications can be seen. In models 1 and 2, duct inlet-exit area ratios were fixed such that at M = 1.00, mass-flow ratios were 0.83 and 0.87, respectively, based on minimum inlet area. The effect of this small difference on area distribution can be seen in figure 2 to 4.

[redacted]

TEST TECHNIQUE

Each model was boosted to a Mach number of about 1.3 by a 6-inch-diameter solid-fuel rocket motor developing about 6,000 pounds thrust for approximately 3 seconds. The models were launched from a mobile zero-length launcher, as shown in figure 9.

The models were tracked in flight by two radar sets, one of which recorded model position in space while the other recorded velocity, both with respect to time. Radiosondes were used to determine atmospheric conditions throughout the altitude ranges traversed by the model flights.

METHOD OF ANALYSIS

The drag data reported herein were obtained during the decelerating portion of the flight where the model was separated from the booster rocket. The method consisted of differentiation of the velocity with respect to time, correcting for flight-path angle, and calculation of the total drag coefficient by the relationship

$$C_{D_{total}} = -\left(\frac{dV}{dt} + g \sin \gamma\right)\frac{W}{qSg}$$

Where q was determined using the velocity corrected for winds, along with atmospheric conditions as obtained from the radiosonde. A complete analysis of the methods used to reduce these data is contained in reference 1.

External drag was determined from the relationship

$$C_{D_{external}} = C_{D_{total}} - C_{D_{base}} - C_{D_{internal}}$$

where $C_{D_{base}}$ and $C_{D_{internal}}$ were estimated on the basis of unpublished data obtained from similar duct and base configurations. While the estimations involved could conceivably be in error by a fairly large percentage, their magnitude is small in comparison with the external drag, so that the overall percentage error is small.

The external drag coefficient $C_{D_{external}}$ obtained by the above method was used in conjunction with unpublished tunnel data to determine $C_{D_{min}}$ by the relationship

[redacted]

$$C_{D_{min(rocket\ test)}} = C_{D_{external(rocket\ test)}} - \left(C_{D_{tunnel}} - C_{D_{min_{tunnel}}}\right)$$

where $C_{D_{tunnel}}$ was taken at trim lift coefficients corresponding to the values of this test. The maximum probable error in $C_{D_{min}}$ is felt to be less than 0.0010.

No Reynolds number corrections have been made to the data presented herein, since it has been found by correlation that drag data from rocket model tests compared directly with data from similar full-scale configurations show excellent agreement, as is shown in reference 2. Apparently, control-surface gaps and small protuberances such as nonflush rivets, gaps in landing-gear doors, and so forth which are present on production aircraft, offset any drag increments caused by variations in Reynolds numbers between tests of the type presented herein and full-scale airplanes. No corrections have been made for spillage drag. Calculations reveal that these corrections would be small.

DISCUSSION OF RESULTS

Reynolds number (based on mean aerodynamic chord) varied from about 6.5×10^6 at $M = 0.85$ to about 11.5×10^6 at $M = 1.3$ for both models, as shown in figure 10. Figures 11 and 12 show total drag coefficient plotted against Mach number for the basic and modified models, respectively. Estimated internal and base drag (based on unpublished results obtained from telemetered data from rocket models with similar duct and base configurations) are also shown in figures 11 and 12.

Figure 13 shows estimated trim lift for both models. The curve is based on unpublished wind-tunnel data from a nonducted model with unmodified nose, comparable to the unmodified model of this test. The data have been corrected to the center-of-gravity location used in the test reported herein (7 percent M.A.C.). It is felt that model 2 is similar enough to model 1 to justify the use of the trim lift values presented in figure 13 for the purpose of estimating drag due to lift. Figure 14 shows the increment between drag corresponding to the trim lift of this test and minimum drag, based on unpublished tunnel data.

Shown in figure 15 is $C_{D_{min}}$ for both models 1 and 2 (the original configuration and the model with modified forebody, respectively). Model 1 had a minimum drag coefficient which increased from 0.0175 at $M = 0.9$ to about 0.0445 at $M = 1.1$, then decreased slightly to 0.0440 at $M = 1.285$. For model 2, the corresponding values were 0.0185, 0.0420, and 0.0410, respectively. For both models the drag rise began at $M = 0.93$, based on $dC_D/dM = 0.10$.

[redacted]

Figure 15 shows that the nose modifications of model 2, while not extreme in nature (see figs. 2 to 8), resulted in decreases of 0.0025 and 0.0030 in the minimum drag coefficient at Mach numbers of 1.1 and 1.285, respectively. The small increase (0.0010) at $M = 0.9$ is probably within the experimental accuracy at subsonic speeds.

Figure 16 shows the variation of pressure-drag coefficient with Mach number. A comparison of the test values (based on zero pressure drag at $M = 0.9$) shows an increment of about 0.0035 between models 1 and 2 at Mach numbers between 1.1 and 1.285. Calculated values, based on the method discussed in reference 3, show an increment of 0.0032. Hence, it is significant that while the method of reference 3 does not predict the pressure drag of a configuration of this type, it does predict the increment in pressure drag occurring from the small modifications in area distribution of model 2 as compared with model 1. This has been observed to be the case in other similar (45° swept wing) configurations.

CONCLUSIONS

From the test of two 0.11-scale rocket-powered models of the Chance Vought XF8U-1 airplane at Mach numbers between 0.85 and 1.30 and at Reynolds numbers between about 6.5×10^6 and 11.5×10^6, respectively, the following conclusions are indicated:

1. The minimum drag coefficient of the first (original) configuration increased from about 0.0175 at $M = 0.9$ to about 0.0445 at $M = 1.1$, then decreased slightly to about 0.0440 at $M = 1.285$. For the second (modified nose) configuration, the corresponding values were 0.0185, 0.0420, and 0.0410. For both configurations, the drag-rise Mach number (based on $dC_D/dM = 0.10$) was 0.93.

2. The nose modifications resulted in a decrease of about 0.0035 in the pressure-drag coefficient at Mach numbers between 1.1 and 1.285.

Langley Aeronautical Laboratory,
National Advisory Committee for Aeronautics,
Langley Field, Va., June 3, 1954.

Willard S. Blanchard, Jr.
Aeronautical Research Scientist

Approved: Joseph A. Shortal
Joseph A. Shortal
Chief of Pilotless Aircraft Research Division

cg

REFERENCES

1. Wallskog, Harvey A., and Hart, Roger G:: Investigation of the Drag of Blunt-Nosed Bodies of Revolution in Free Flight at Mach Numbers From 0.6 to 2.3. NACA RM L53D14a, 1953.

2. Purser, Paul E.: Comparison of Wind-Tunnel, Rocket, and Flight Drag Measurements for Eight Airplane Configurations at Mach Numbers Between 0.7 and 1.6. NACA RM L54F18, 1954.

3. Nelson, Robert L., and Stoney, William E., Jr.: Pressure Drag of Bodies at Mach Numbers up to 2.0. NACA RM L53I22c, 1953.

[redacted]

TABLE I.- GEOMETRIC DIMENSIONS

	Model 1	Model 2
Wing:		
Total area, sq ft	4.55	4.55
Exposed area, sq ft	3.61	3.61
Aspect ratio	3.40	3.40
Sweepback (quarter chord), deg	42	42
Taper ratio	0.27	0.27
Airfoil at root (free stream)	NACA 65A006	
Airfoil at tip (free stream)	NACA 65A005	
Dihedral, deg	-5	-5
Incidence, deg	-1	-1
Horizontal tail:		
Total area, sq ft	1.28	1.28
Exposed area, sq ft	0.84	0.84
Aspect ratio	3.49	3.49
Sweepback (quarter chord), deg	42	42
Taper ratio	0.15	0.15
Airfoil at root (free stream)	NACA 65A006	
Airfoil at tip (free stream)	NACA 65A004	
Dihedral, deg	5.4	5.4
Incidence, deg	0	0
Vertical tail:		
Total area (to center line), sq ft	1.24	1.24
Exposed area, sq ft	0.98	0.98
Aspect ratio (exposed)	1.14	1.14
Sweepback (quarter chord), deg	42	42
Taper ratio	0.31	0.31
Airfoil at root (free stream)	NACA 65A006	
Airfoil at tip (free stream)	NACA 65A004	
Fuselage:		
Frontal area, sq ft	0.31	0.31
Length, ft	5.58	5.62
Base area, sq ft	0.07	0.07
Fuselage nose to wing leading edge at center line, ft	1.97	2.00
Fuselage nose to horizontal-tail leading edge at center line, ft	4.51	4.54
Center-of-gravity location, percent $\bar{c}$	0.07	0.07
Duct-inlet area, sq ft	0.049	0.052
Duct-exit area, sq ft	0.044	0.049

[redacted]

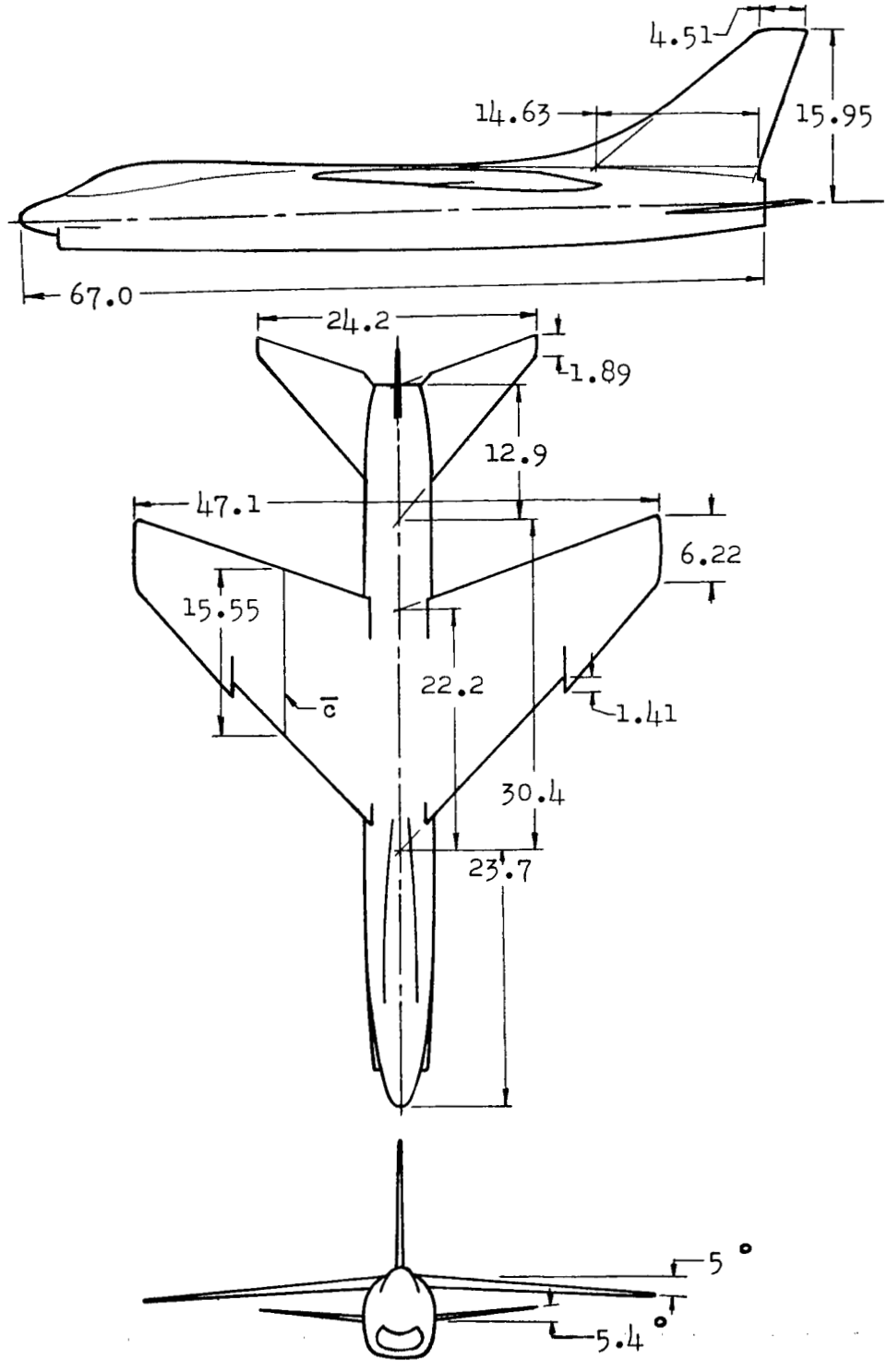

Figure 1.- Three-view drawing of the basic (unmodified) model. All dimensions are in inches unless otherwise noted.

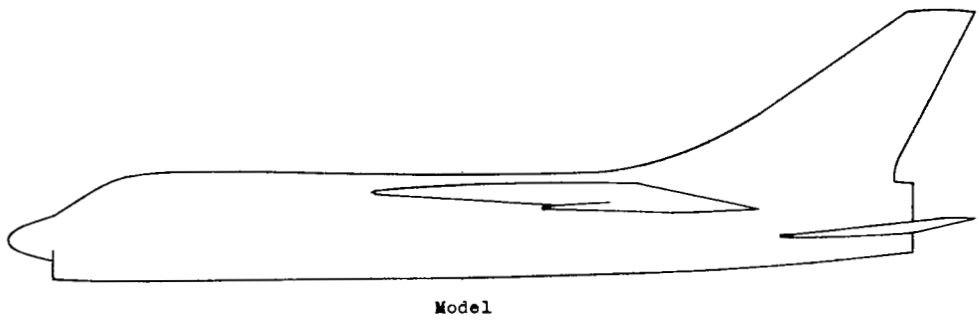

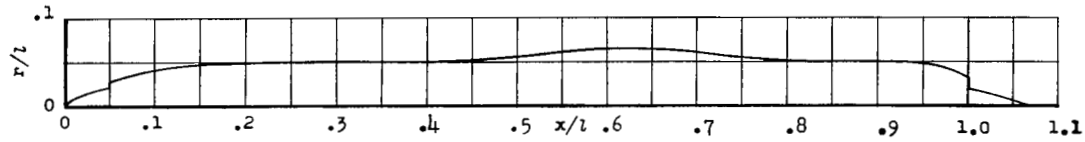

(a) Equivalent body (complete model).

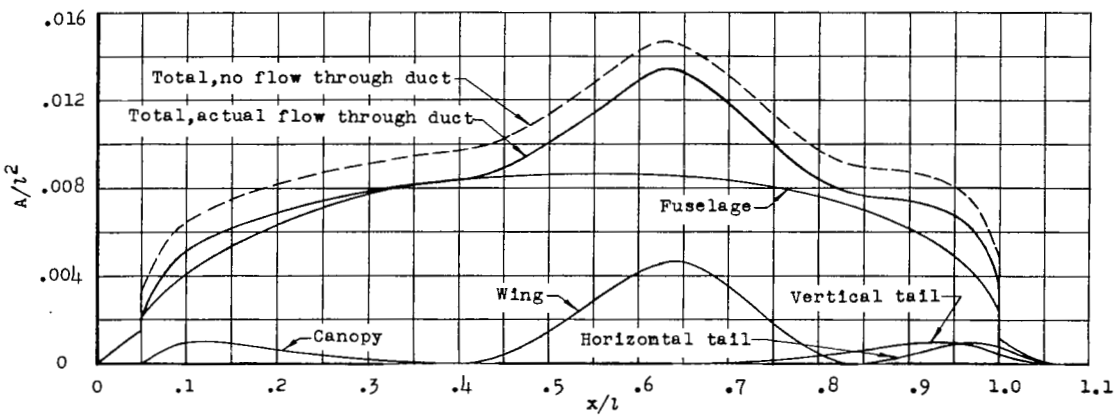

(b) Breakdown of areas of the components.

Figure 2.- Nondimensional area distribution of the basic model.

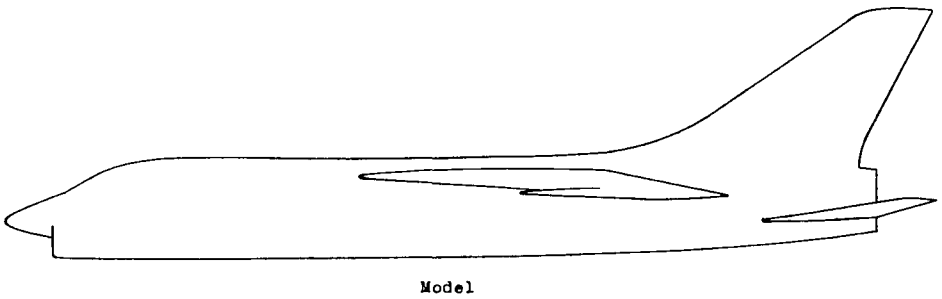

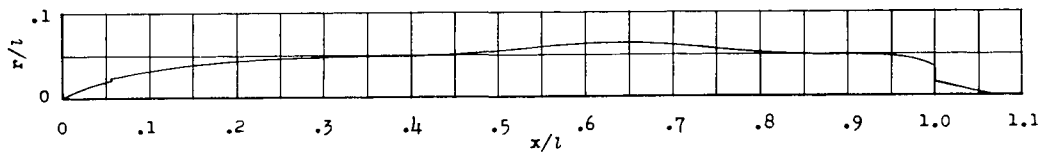

(a) Equivalent body (complete model).

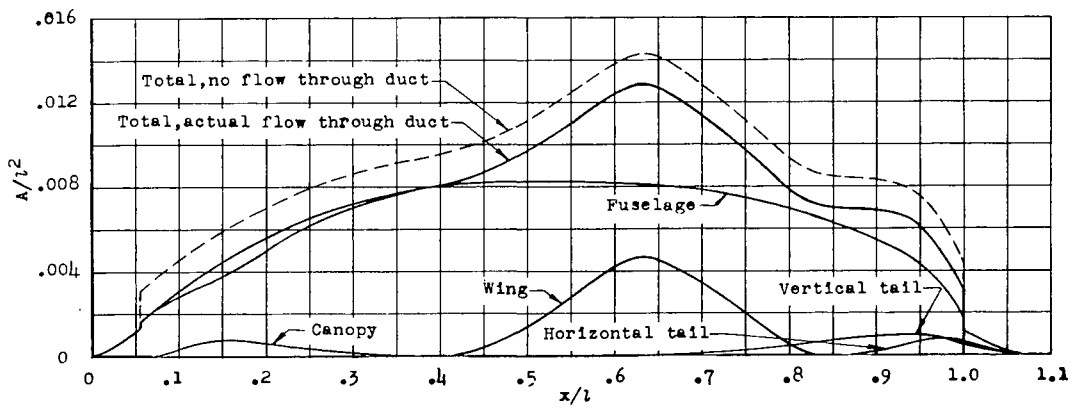

(b) Breakdown of areas of the components.

Figure 3.- Nondimensional area distribution of the model with nose modifications.

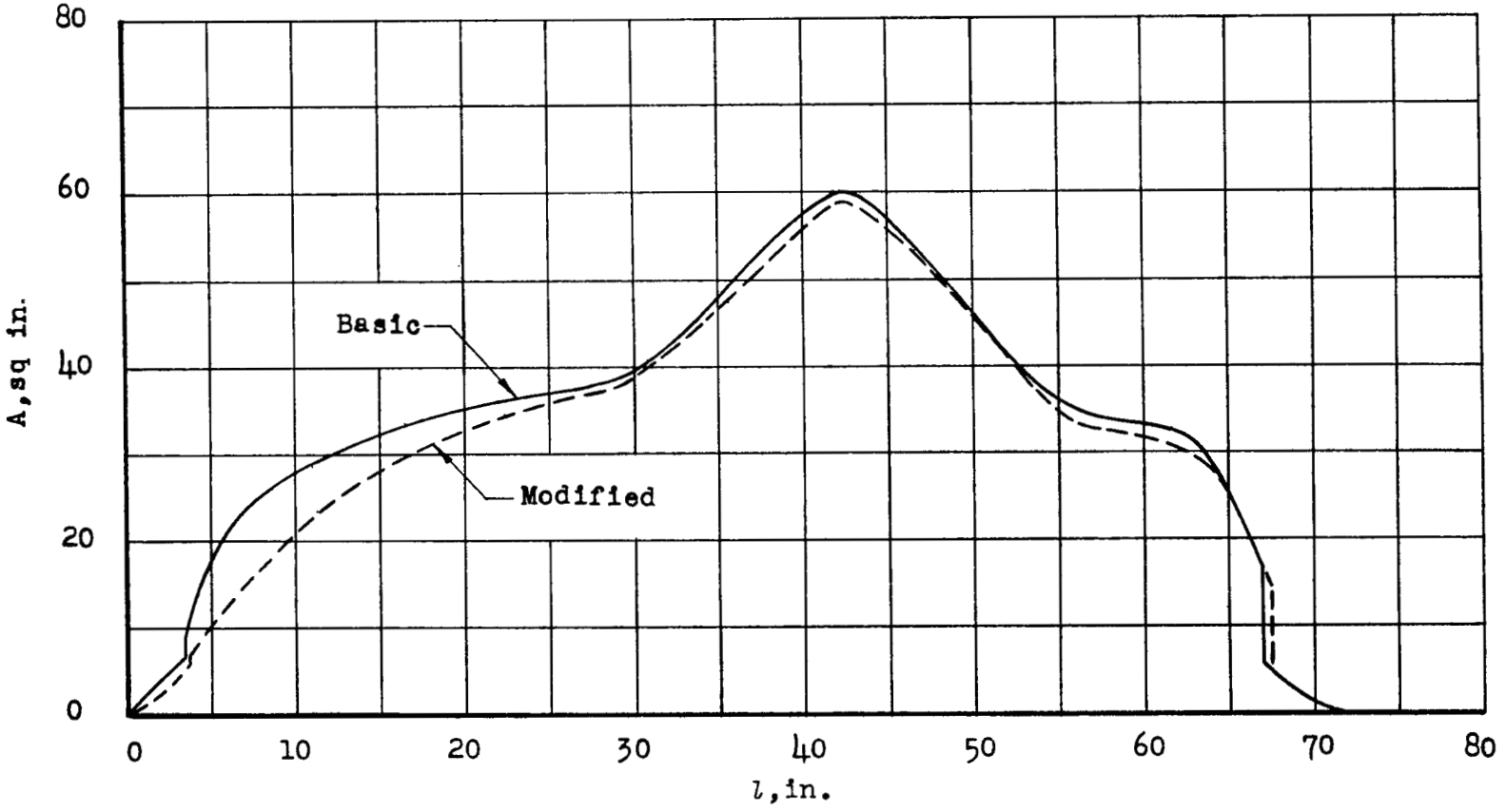

Figure 4.- Dimensional area distribution of the basic configuration and the model with nose modifications (both with actual flow through duct).

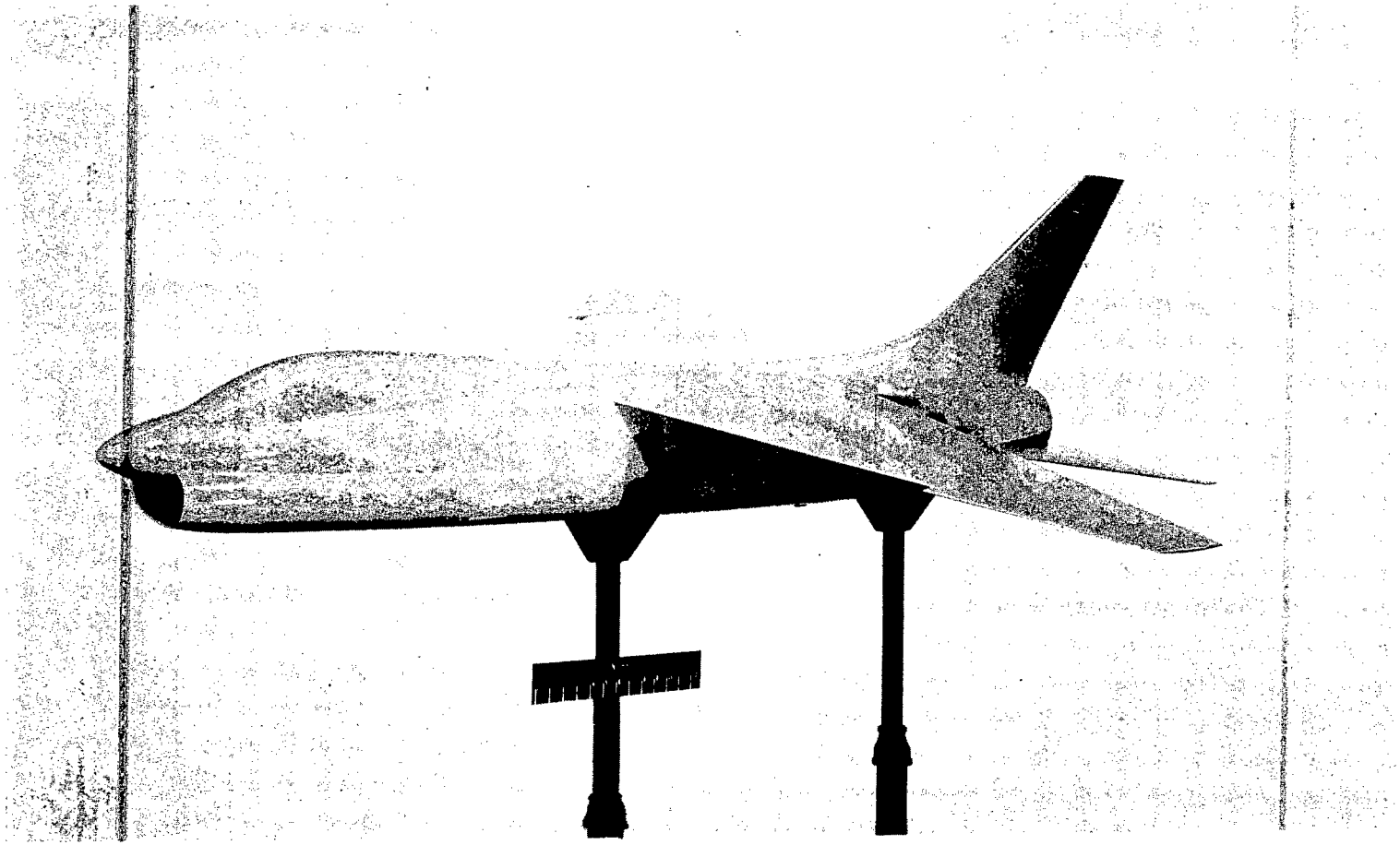

L-81834.1

Figure 5.- Three-quarter front view of the basic configuration.

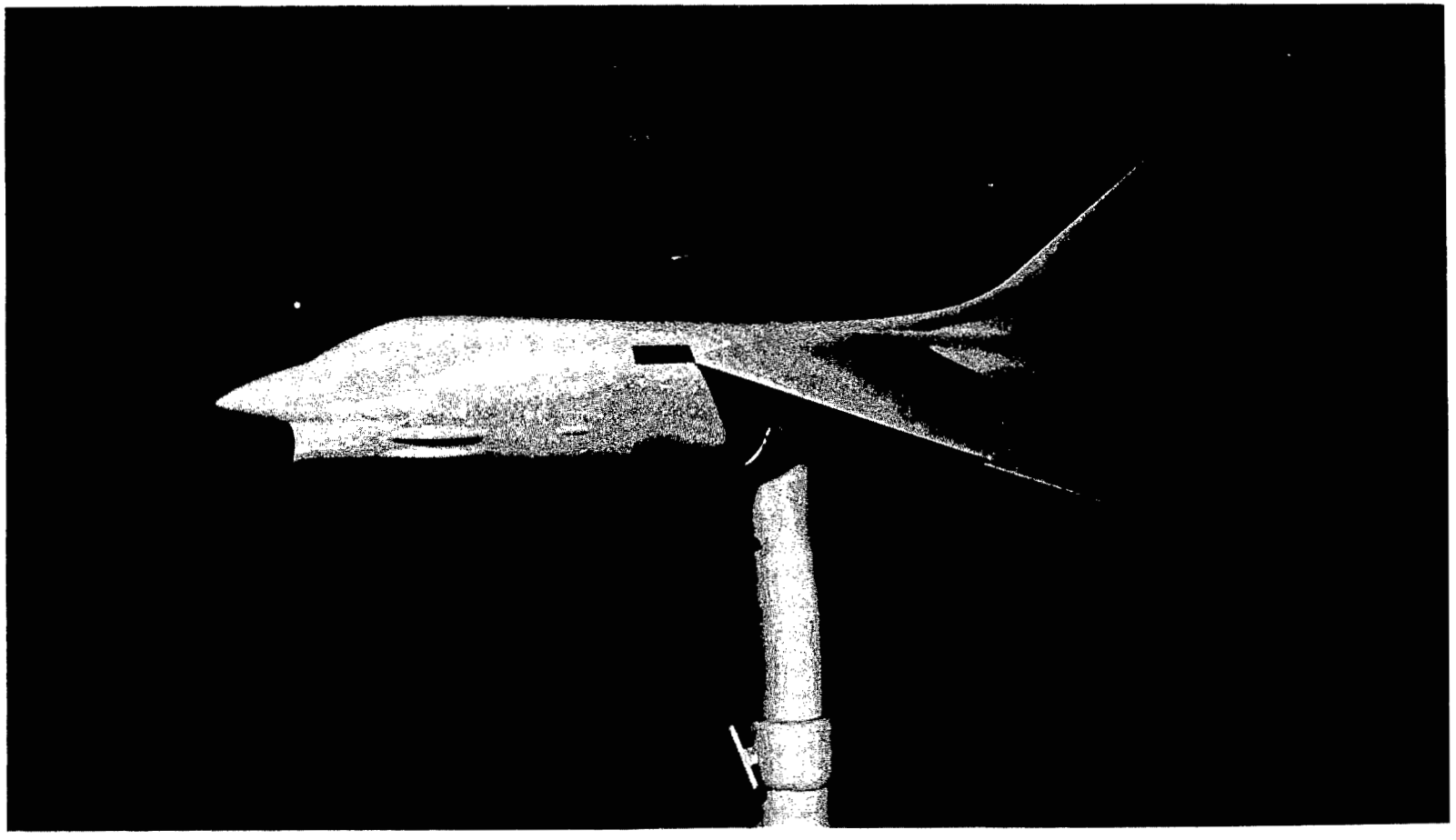

L-82838

Figure 6.- Three-quarter front view of the model with nose modifications.

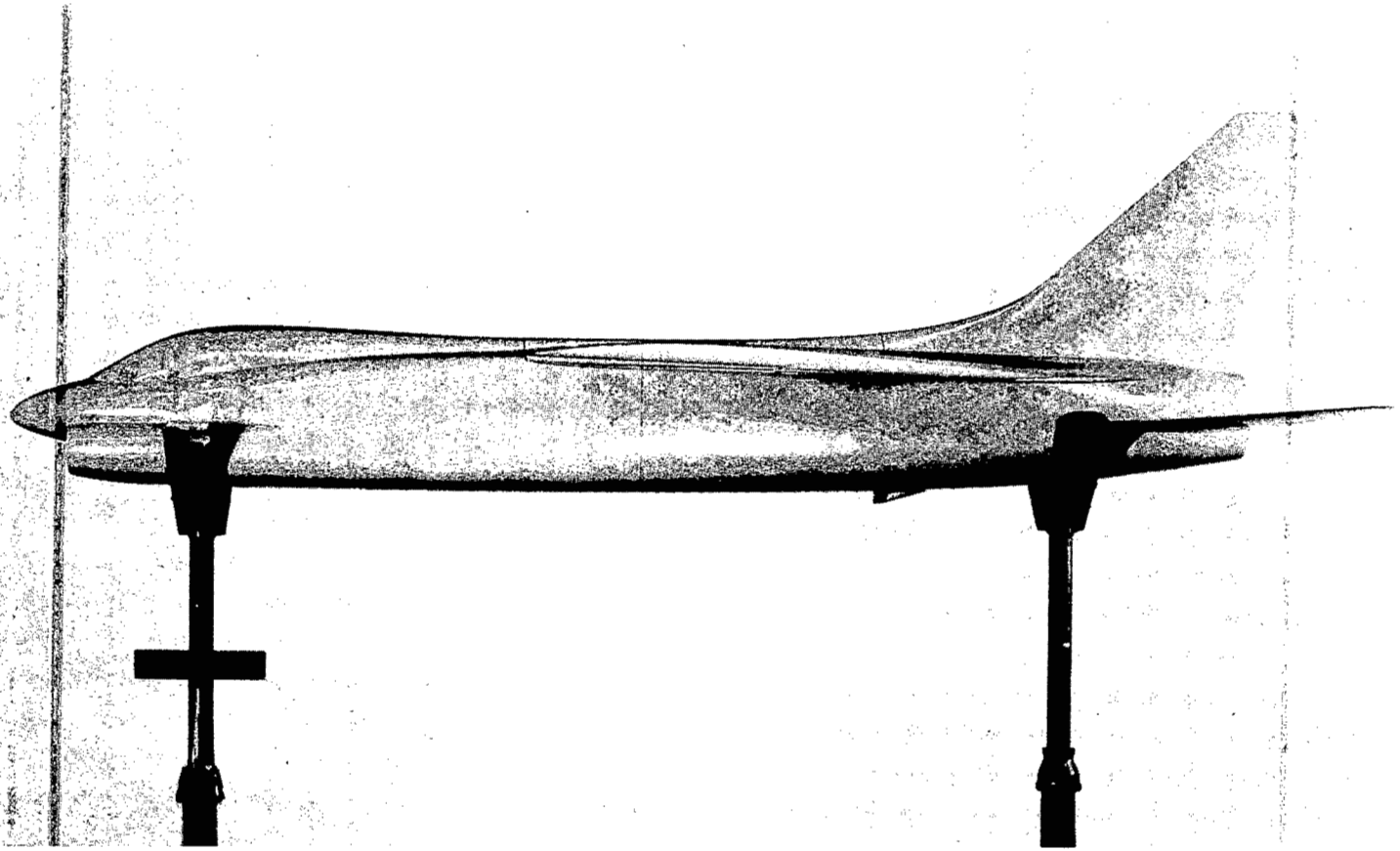

L-82170.1

Figure 7.- Side view of the basic configuration.

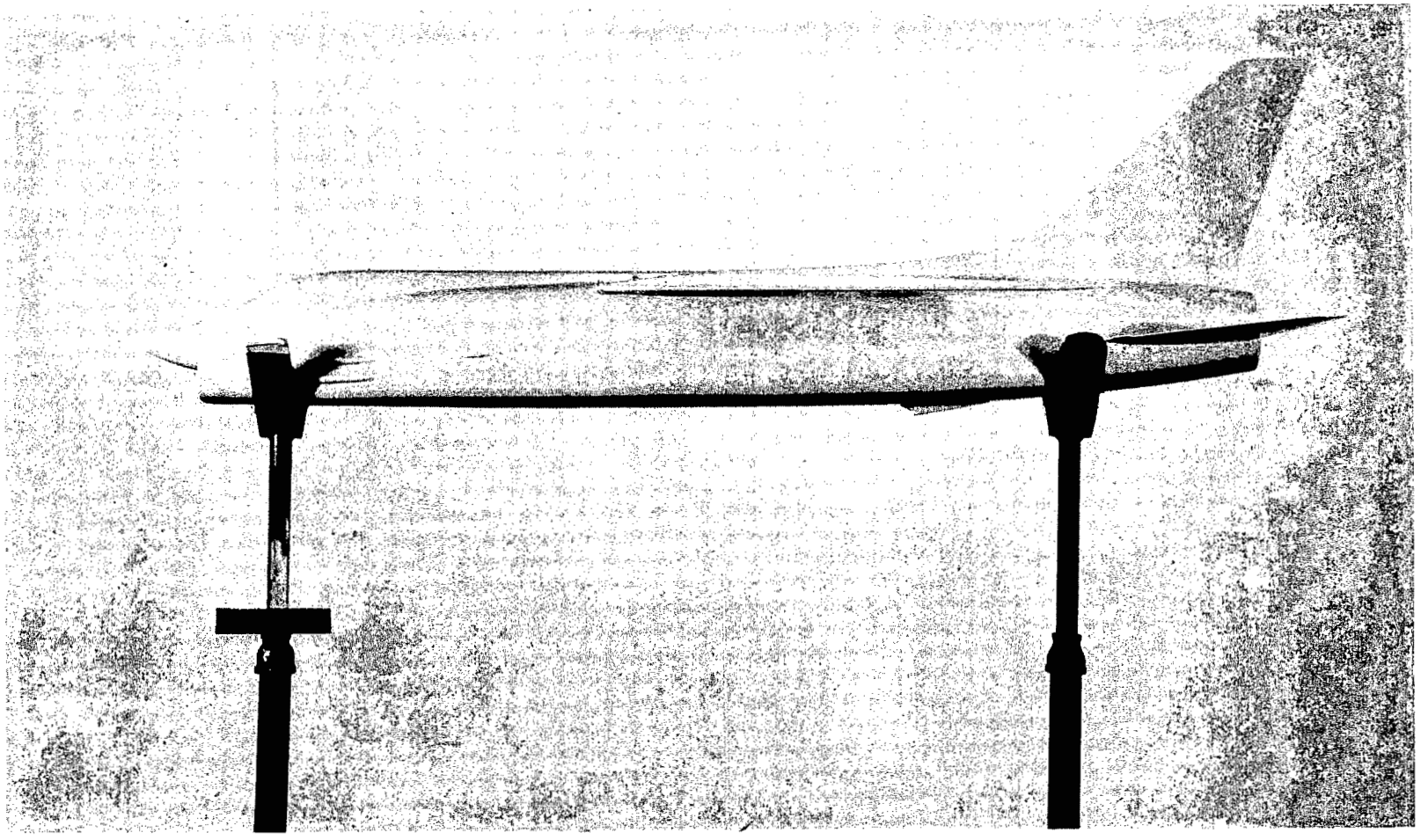

L-82902.1

Figure 8.- Side view of the model with nose modifications.

L-82484

Figure 9.- One of the model-booster combinations in launching position.

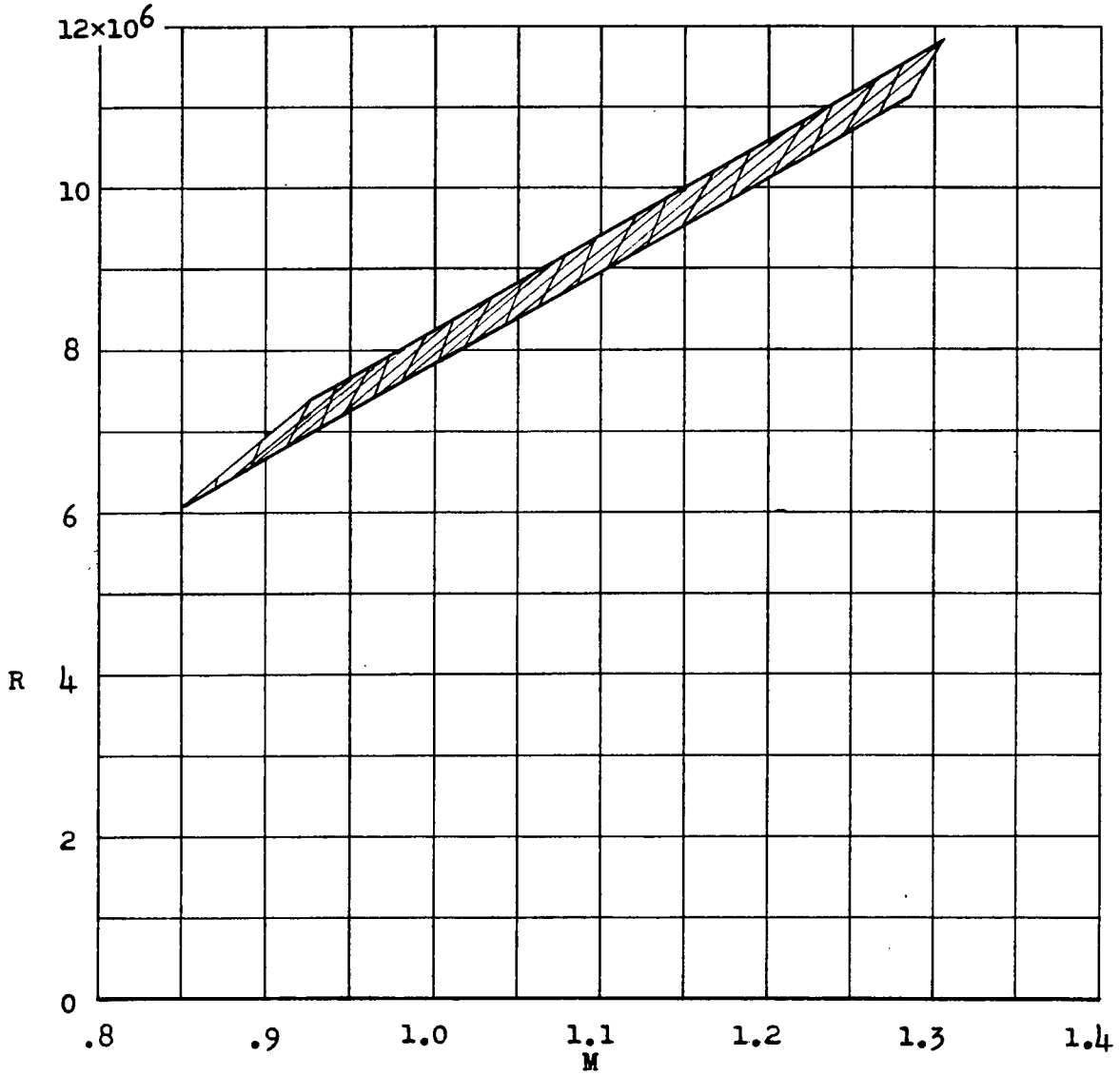

Figure 10.- Variation of Reynolds number with Mach number.

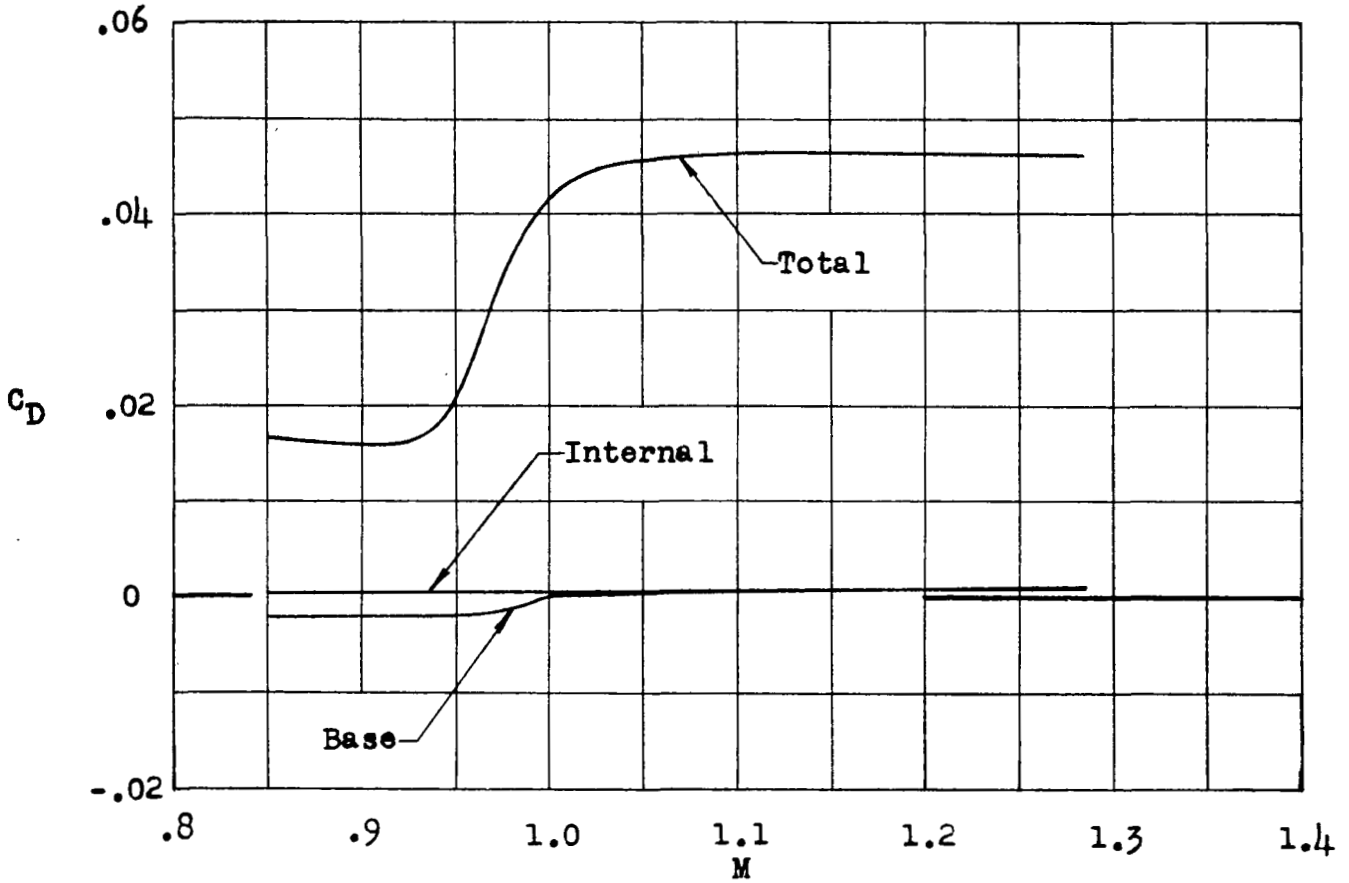

Figure 11.- Total, internal, and base drag of the basic configuration.

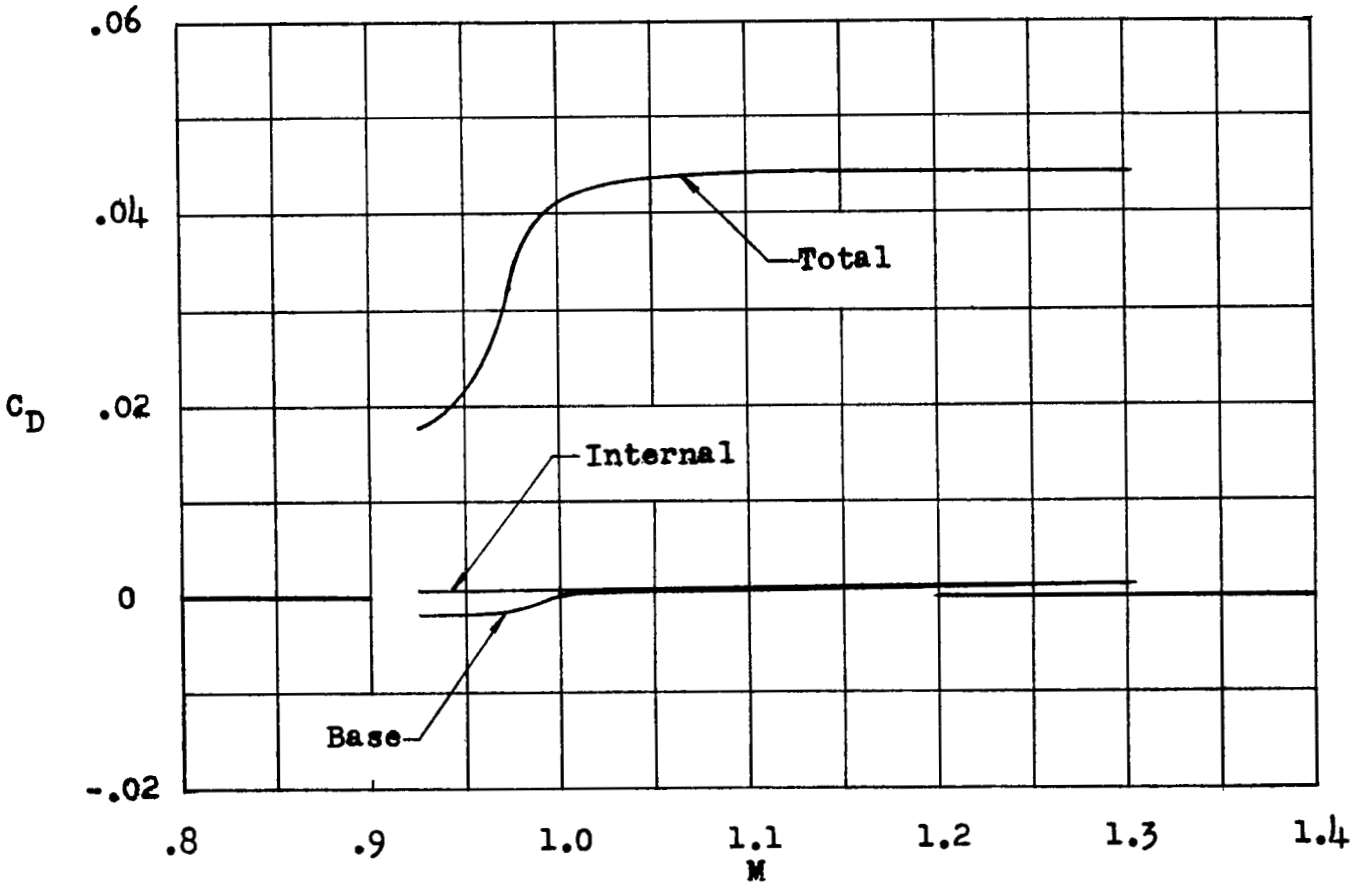

Figure 12.- Total, internal, and base drag of the model with forebody modifications.

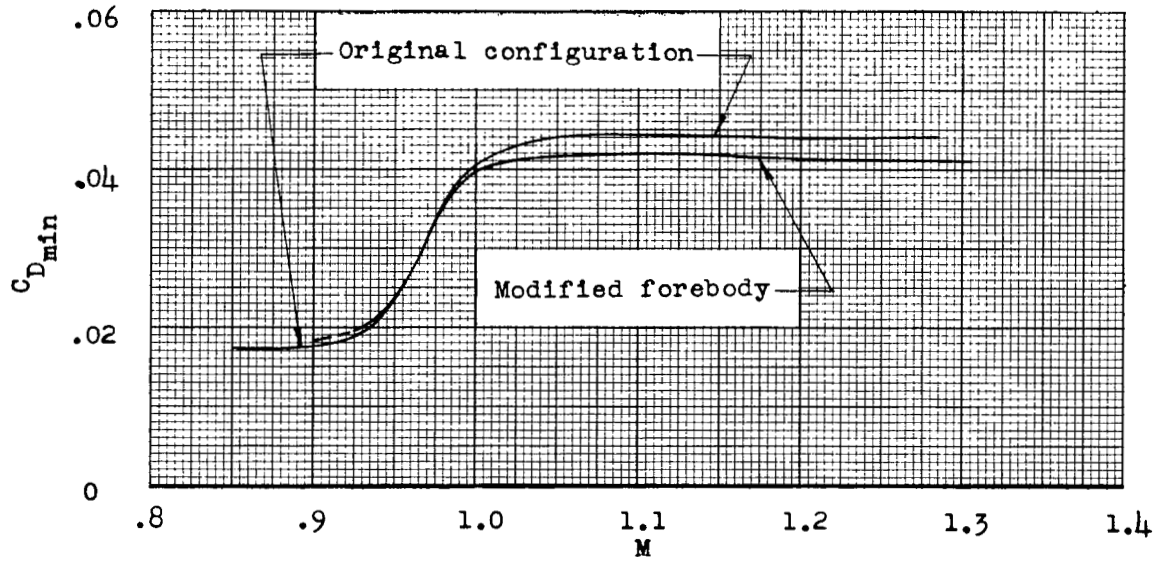

Figure 15.- Minimum drag coefficient.

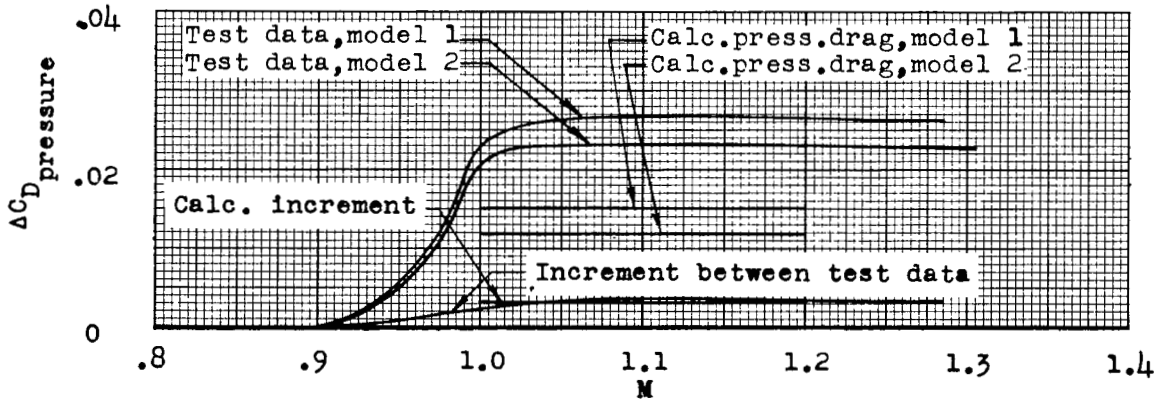

Figure 16.- Pressure-drag coefficient; calculated values are shown over a Mach number range for illustrative purposes.

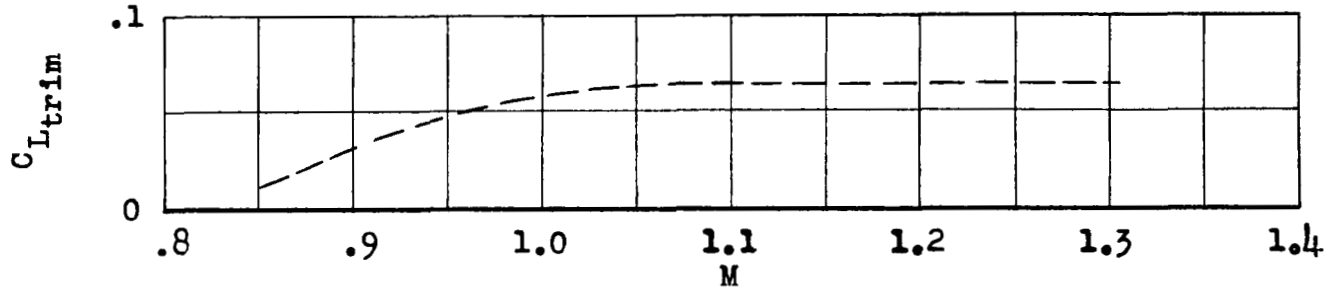

Figure 13.- Estimated trim lift (based on unpublished tunnel data, extrapolated above M = 1.15).

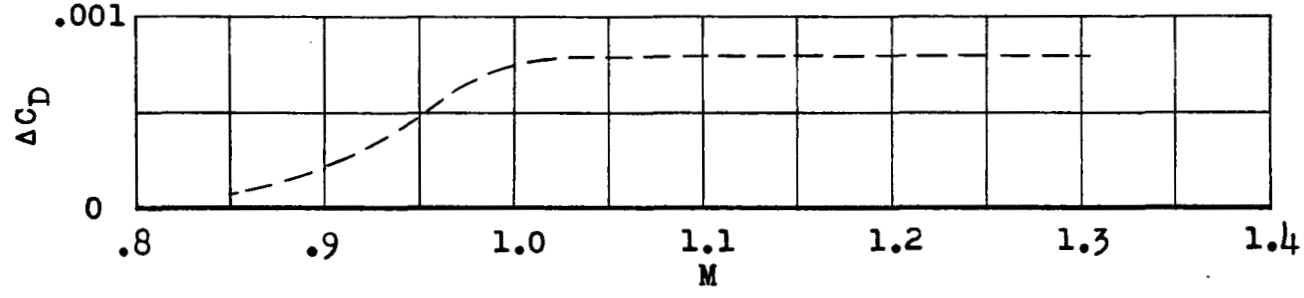

Figure 14.- Increment between minimum drag coefficient and drag coefficient at the trim lift of this test (based on unpublished tunnel data, extrapolated above M = 1.15).